Earth and Space Science

RESEARCH ARTICLE
10.1029/2021EA002122

Special Section:
Science Results from NASA's Solar Irradiance Science Team #2 (SIST-2) Program

SORCE and TSIS-1 SIM Comparison: Absolute Irradiance Scale Reconciliation

Jerald Harder[1], Stéphane Béland[1], Steven V. Penton[1], Erik Richard[1], Elizabeth Weatherhead[2], and Eduardo Araujo-Pradere[3]

[1]Laboratory for Atmospheric and Space Physics, University of Colorado, Boulder, CO, USA, [2]Jupiter Intelligence, Boulder, CO, USA and University of Colorado (retired), Boulder, CO, USA, [3]Department of Mathematics and Science, Miami Dade College, Miami, FL, USA

Key Points:

- Conduct a comparison of Solar Radiation and Climate Experiment (SORCE) and Total and Spectral Irradiance Sensor (TSIS-1) Spectral Irradiance Monitors (SIM) over a 705-day time period
- Construct a multiplicative correction factor that brings the SORCE SIM into agreement with the pre-flight calibration of TSIS-1 SIM
- Characterize the uncertainties associated with the correction factor—uncertainty was two orders of magnitude less than the correction

Correspondence to:
S. Béland,
stephane.beland@lasp.colorado.edu

Citation:
Harder, J., Béland, S., Penton, S. V., Richard, E., Weatherhead, E., & Araujo-Pradere, E. (2022). SORCE and TSIS-1 SIM comparison: Absolute irradiance scale reconciliation. *Earth and Space Science*, *9*, e2021EA002122. https://doi.org/10.1029/2021EA002122

Received 20 NOV 2021
Accepted 11 JAN 2022

Author Contributions:
Conceptualization: Jerald Harder, Stéphane Béland, Erik Richard, Elizabeth Weatherhead
Data curation: Steven V. Penton
Formal analysis: Jerald Harder, Stéphane Béland, Steven V. Penton, Elizabeth Weatherhead
Funding acquisition: Jerald Harder, Stéphane Béland
Investigation: Jerald Harder, Steven V. Penton, Elizabeth Weatherhead, Eduardo Araujo-Pradere

Abstract The Solar Radiation and Climate Experiment (SORCE) and Total and Spectral Irradiance Sensor (TSIS-1) conducted an intercomparison for the two Spectral Irradiance Monitors (SIM) spanning 704 days from 23 March 2018 to 25 February 2020 and permitted 554 time-matched pairs of observations. This comparison was conducted during the extremely quiescent Solar Cycle 24 minimum, so all observed differences and drifts between the two sensors are instrumental in nature. The TSIS-1 SIM benefitted from advanced calibration capabilities based on SI standards that were not available during the preflight calibration time period of SORCE. For this reason, a revision of the SORCE SIM absolute scale is appropriate. As expected, wavelength dependent differences in absolute agreement are a function of detector sensitivity and local changes in spectral slope. At the time of the comparison SORCE SIM has been on-orbit for 17 years while TSIS-1 observations commenced immediately after a 100-day outgassing and commissioning period. Peak-to-peak absolute scale differences are about 12% with a mean fractional difference of 0.7% ± 2.9%. The greatest scale differences occur at the change-over between the UV and visible photodiodes in the 310 nm region, and a systematic disagreement is present in the 850–1,600 nm range. A multiplicative scale correction factor has been developed to reconcile the TSIS-1 and SORCE difference with a wavelength dependent error on the mean typically less than 0.01% derived from every matched pair of observations.

1. Introduction

Solar irradiance variability is put into the context of Earth atmospheric anthropogenic and natural climate forcing in Chapter 2 of the Fourth Assessment Report of the Intergovernmental Panel on Climate Change (IPCC; Forster et al., 2007). In this report, the authors estimate that the combined radiative forcing due to anthropogenic contributions [+1.6 (−1.0, +0.8) W m^{-2}] is likely to be at least five times larger than the secular change in the total solar irradiance (TSI) since the dawn of the industrial age in the year 1750. However, the report ranks the scientific understanding of the solar contribution as "low" and notes that additional climate forcing through the Sun's ultraviolet (UV) contributions and other solar related mechanisms such as energetic particle deposition in the upper atmosphere cannot be ruled out (Seppälä & Clilverd, 2014). The review of solar forcing in the Earth's atmosphere by Gray et al. (2010) delineates a number of potential mechanisms that might contribute significantly to the Earth climate observations that were beyond the scope of the IPCC report. Both the Gray et al. (2010) review and the IPCC assessment emphasize what can be learned from proxy-based studies of solar variability; this is a very natural tendency since long-term records are needed to discern the lowest-frequency modes of the solar forcing component (Douglass & Clader, 2002).

For about a decade, in-depth studies involving stratospheric chemistry climate models have included solar spectral irradiance (SSI) variations. In depth chemistry-climate model comparison studies reported by Austin et al. (2008); Mattthes et al., 2017 (CMIP6); and Mitchell et al., 2015 (CMIP5). These detailed studies suggest not only direct photochemical response to UV variability in the stratosphere, but a solar-induce dynamical response. In the CMIP5 Study (Mitchell et al., 2015) suggested solar cycle modification of the Polar Jet Oscillation, but the model response was not robust across all the models employed in the study. Dhomse et al. (2016) conducted a similar study with reanalyzed SAGE observations but noted that, even with improvements in the SAGE II data, there are still large uncertainties in current observational and meteorological reanalysis data sets that require a more accurate quantification of the solar influence than what is currently existent.

This crucial quantification of the solar influence for SSI involves two interlinked activities. First, the absolute radiometric scale of the spectral radiometer must be established and comply with international standards, and

Methodology: Jerald Harder, Stéphane Béland, Steven V. Penton, Elizabeth Weatherhead
Project Administration: Stéphane Béland
Software: Stéphane Béland, Steven V. Penton
Supervision: Jerald Harder, Stéphane Béland
Validation: Jerald Harder, Stéphane Béland, Steven V. Penton, Erik Richard, Elizabeth Weatherhead, Eduardo Araujo-Pradere
Writing – original draft: Jerald Harder, Stéphane Béland, Steven V. Penton, Elizabeth Weatherhead
Writing – review & editing: Jerald Harder, Stéphane Béland, Steven V. Penton

second, the stability of the instrument must be analyzed to assess potential long-term drifts in the instrument induced by potential uncorrected sensitivity degradation. This second point is crucial because the required climate records of solar variability must span multiple missions and several solar cycles. Section 2 sets the stage for the comparative analysis by comparing and contrasting Solar Radiation and Climate Experiment (SORCE) and Total and Spectral Irradiance Sensor (TSIS-1) Spectral Irradiance Monitors (SIM) instrument attributes, generational differences in instrument design, and the status of the two instruments at the time of the comparison. Section 3 provides the detailed statistical analysis used to derive the TSIS-1 SIM Adjusted Values (TAV) presented in Section 4. This wavelength-dependent one-time irradiance scale correction essentially updates the original SORCE ALEPH correction, but at the end of the mission instead of SORCE DAY 453 (21 April 2004). This irradiance correction does not attempt to correct any long-term trends present in the SORCE SIM V27 and TSIS-1 SIM V06 data. A consistent degradation correction method is applied uniformly throughout the SORCE mission (Harder et al., 2021). Once these degradation corrections are made, the final step is to apply a multiplicative correction factor to bring the SORCE data onto the irradiance scale of the SORCE SIM reference spectrum determined on mission day 453 as described in Harder et al. (2010). In essence what we are doing in this manuscript is to bring this SORCE DAY 453 reference spectrum into agreement with preflight calibration of TSIS-1. The TSIS-1 corrected SORCE SIM data along with its associated uncertainties is published on the SORCE website (see Section 6 for the necessary links). Section 5 then compares the integrated TAV data product with SORCE TIM V19 TSI. Section 6 specifies all the online locations of critical data that is used in the overlap analysis. Section 7 summarizes the results and discusses the impact of the advanced calibration capabilities of TSIS-1 SIM. Assessment of the mutual long-term stability of the two instruments is presented in a separate manuscript in this journal.

2. Basis for the SORCE and TSIS-1 Instrument Comparison

2.1. Summary of SORCE and TSIS-1 Instrument Attributes

The design, operation, calibration, and performance of SORCE SIM is described in a series of papers published in the journal *Solar Physics*. The first (Harder, Fontenla, et al., 2005) describes the scientific requirements, design, and operation modes for the instrument. The second (Harder, Fontenla, et al., 2005) discusses the fundamental measurement equations and the preflight calibration methodology for the instrument. The third paper (Harder et al., 2010) continues the discussion of the absolute calibration of the instrument describing additional post-launch characterizations using flight spare components and comparisons with the SORCE and UARS Solar Stellar Irradiance Comparison Experiment (SOLSTICE) instruments and the ATLAS 3 composite (Thuillier et al., 2009). A comprehensive discussion of SORCE SIM degradation corrections and the method used to extract time dependent errors is presented in Harder et al. (2021).

Harder, Fontenla, et al. (2005) provides a detailed description of the SIM instrument, but the basic optical configuration is briefly described here. There are two SIM channels called SIMA and SIMB. SIMA is used for daily solar measurements, and SIMB is used for tracking SIMA degradation trends and only makes solar observations about once a month. Each SIM channel has an entrance slit, a Féry prism, and a set of exit slits for each detector in its focal plane. There are three different photodiodes to cover the wide SIM spectral range of 200–1,630 nm and referred to as the UV, VIS1, and IR photodiodes. The reference detector for each channel is an electrical substitution radiometer (ESR) that provides a very low degradation irradiance measurement standard and is used to correct the more radiation susceptible photodiode detectors. The ESR also provides measurements for the IR out to 2,416 nm.

Richard et al. (2020) provide a detailed analysis and description of the TSIS-1 SIM instrument and its preflight calibration. TSIS-1 SIM began operations from the International Space Station (ISS) in March 2018 and nominally provides an SSI spectrum every 12 hr. Advances in both instrument design and preflight spectral irradiance calibration techniques have resulted in the TSIS-1 SIM achieving higher absolute accuracy than the first generation SORCE SIM throughout the 200–2401.4 nm spectral range. A comprehensive detector-based Spectral Radiometer Facility (SRF) was developed in collaboration with the US National Institute for Standards and Technology (NIST) to ensure compliance to spectral SI standards in power and irradiance. Traceability is achieved via direct laser calibration of a focal plane ESR against a cryogenic radiometer in power mode and also irradiance responsivity via calibrated apertures. The TSIS-1 SIM accuracy definition followed an absolute sensor approach based on a full radiometric measurement equation where component-level performance characterizations and calibrations were quantified with an associated uncertainty error budget and verified by independent

measurements for each parameter. Unit-level characterizations were completed over the full operational envelope of external driving factors (e.g., pointing and temperature ranges) and were allowed for the independent parameterization of sub-assembly performance for expected operating conditions. Validation and final instrument end-to end absolute calibration in the Laboratory for Atmospheric and Space Physics (LASP)-SRF achieved low combined standard uncertainty ($u_c < 0.25\%, k = 1$) in spectral irradiance.

2.2. TSIS-1 Instrument Design Enhancements From the SORCE Design

The TSIS-1 SIM was launched with an absolute scale calibration traceable to SI standards with an overall uncertainty of ~0.1%–0.25%—about a factor of 10× improvement over available calibration capabilities at the time of the SORCE preflight calibration (2001–2003). Improvements in absolute scale accuracy where driven by the NIST development of the Spectral Irradiance and Radiance Calibration using Uniform Sources (SIRCUS; Brown et al., 2004) laser system in conjunction with a NIST calibrated cryogenic radiometer. Additional design improvements and lessons-learned between the SORCE and TSIS-1 eras include:

1. Provide an ultra-high vacuum/ultra clean instrument chamber design that limits hydrocarbon contamination of the prism glass – the leading cause of degradation in satellite-borne spectral spectrometers.
2. Employ a three-spectrometer redundancy instead of two that allows for improved degradation corrections for both the daily working channel (SIMA) and the monthly correction channel (SIMB).
3. Conduct instrument operations that follow strict non-varying rates of solar exposure.
4. Redesign ESR for improved low-noise performance. A reduced ESR bolometer capacitance increases the open-loop gain thereby increasing detector sensitivity.
5. TSIS-1 SIM photodiodes employ 20 bit dual-slope analog-to-digital converter (ADC) compared to a 13-bit sampled ADC on SORCE—an improvement of factor of 128 thereby permitting photon noise limited performance of these detectors.
6. Improved stray light rejection and off-axis pointing corrections.

2.3. Instrument Status at the Time of the Comparison

2.3.1. Challenges in the SORCE/TSIS-1 Comparison

It is important to note that the comparison was conducted during the last two years of the SORCE 17-year mission, while the TSIS-1 observations commenced shortly after commissioning (on TSIS-1 mission day 100). Because of this, SORCE and TSIS-1 are in entirely different states of degradation and employ very different methods of degradation correction. In particular, the accumulated amounts of solar exposure are vastly different on the last day of the overlap period. For SORCE the SIMA channel had 461.9 days of exposure, and SIMB had a total 75.4 days. For TSIS-1, its three channels were 75.3, 8.8, and 1.0 days of exposure at the end of the comparison time period. Note that analysis of telemetry provides very accurate measures of exposure time, and this quantity is a key component in the degradation correction schemes for both instruments.

Another important point is that the observation schedules for these two instruments were very different particularly during the time of this comparison for the SORCE instrument. By September 2010 (7.6 mission years) management of the SORCE battery power due to the inevitable failure of the nickel hydride common pressure vessel (CPV) battery cells dictated every-orbit power cycling first for SIMB in September 2010 and then both SIM channels in May 2011. In July 2013 (10.5 mission years), two additional CPV failures caused the battery voltage to drop below the brownout threshold for the primary onboard computer (OBC) during eclipse periods. The SORCE Mission Operation team developed a process to manually turn on the OBC at orbit sunrise, then load and execute stored commands to turn on the remaining components during orbit day and off again prior to sunset. This process relied on Tracking and Data Relay Satellite System (TDRSS) satellite-to-satellite communication to both command and collect SORCE telemetry. This highly complex mission scenario is referred to as the Day-Only Operation (DO-Op) mode in this document. As discussed in subsequent sections, daily corrections are made for wavelength shift and temperature drift—see Section 2.3.2. An additional correction is needed for time periods of telemetry blackout where communications with the TDRSS satellite were disrupted. In a similar manner, TSIS-1 SIM acquires data over several orbits to maintain a constant rate of exposure for all three channels, although ISS activities occasionally interrupt data acquisition.

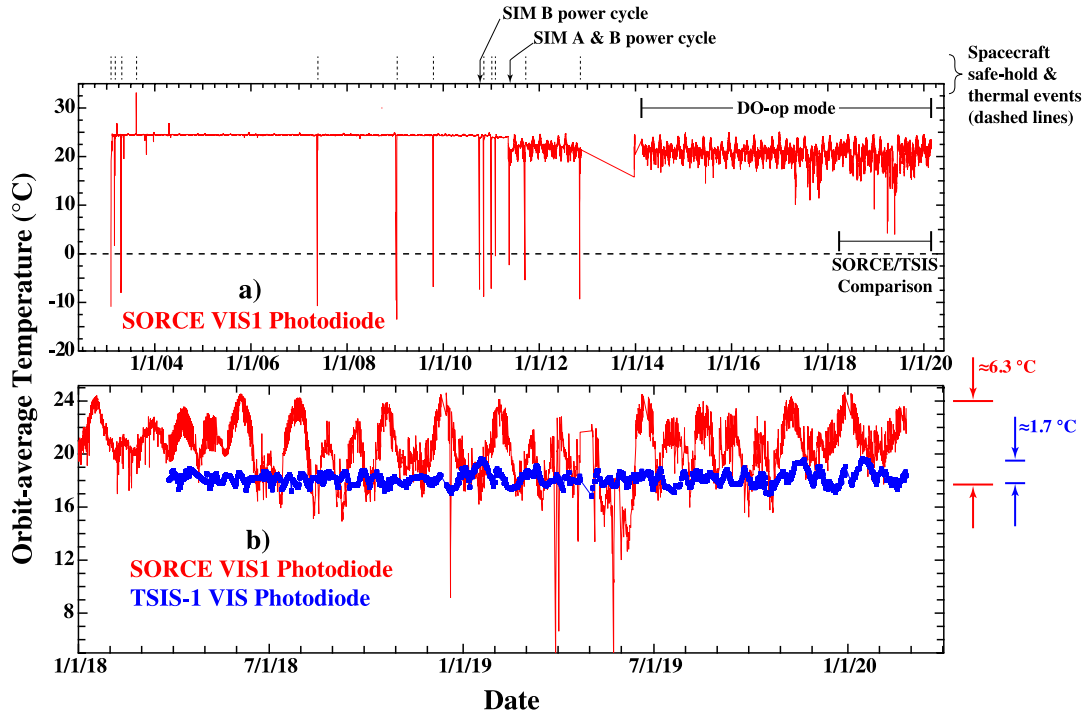

Figure 1. The temperature history for the visible (VIS1) photodiode on both Solar Radiation and Climate Experiment (SORCE) and Total and Spectral Irradiance Sensor (TSIS-1) Spectral Irradiance Monitor. Panel (a) shows the mission length time history for this temperature monitor. The downward spikes seen in the data correspond to spacecraft safe-hold and thermal events. Notice that during the power cycling and Day-Only Operation mode more significant temperature variations occur. Panel (b) shows the temperature variations during the SORCE/TSIS-1 comparison time period and indicates the magnitude of the temperature variations for both instruments.

2.3.2. SORCE/TSIS-1 Temperature History During the Comparison

One of the critical requirements for solar spectral radiometry is to be able to discriminate day-to-day differences in solar irradiance on the order 10^{-4} or better. One of the major hurdles in achieving this level of precision is to autonomously maintain continuous orbit-to-orbit temperature stability to within about 1°C. For both SORCE and TSIS-1, temperature enters the spectral radiometer's measurement equation through changes in the index of refraction of the prism glass, temperature dependence of the radiant sensitivity of the photodiode detectors, and changes in mechanical alignment to critical components in the instrument's optical train. In addition to loss of optical transmissivity due to solar radiation, temperature induced changes in orientation of optical elements, focal plane location of slits, and possibly bending of the optical bench produce irreversible changes in the overall sensitivity of the instruments that require amendments in the measurement equation. This problem is particularly noticeable in SORCE SIM where multiple spacecraft safe-hold events caused instrument temperatures to drop below 0°C for several consecutive days. After these events, noticeable changes in the wavelength scale and detector response were observed that required changes in data processing to correct for the occurrence these events. The problem was exacerbated in SORCE SIM with the transition to the DO-Op mode in April 2014 where instrument power was shut off on every orbit-night to conserve battery power, and instrument heating and observations were restarted upon the return to orbit-day.

The full-mission temperature history of the SIM instrument is shown in Figure 1a, as depicted for the SIMA VIS1 photodiode temperature. Because SIMA and SIMB are located in the same physical enclosure and thermally clamped to the spacecraft observatory, very similar temperature values occur for the two channels. The VIS1 photodiode is located in close proximity to the ESR detector – the only individually heated sub-component in the instrument. Figure 1a shows a clear indication of the safe-hold events where temperatures dropped below 0°C. The time periods of individual orbit night power cycling are identified at the top of the panel. Figure 1b details the temperature variations during the time frame of the SORCE/TSIS-1 comparison and shows a reduction in temperature stability while operating in the DO-Op mode relative to the TSIS-1 SIM under full-time temperature

control. The larger variations are tied to the spacecraft beta-angle that controls the length of time the instruments are in the daylight portion of the orbit. Prior to temperature cycling in the early part of the mission, the SORCE SIM VIS1 temperature monitor has a long-term stability about ~0.4°C peak-to-peak variations—this is to be compared to TSIS-1 SIM where the variations are about 1.7°C. When power cycling commenced on SORCE SIM, the beta-angle related temperature variations increased to ~6.3°C thereby reducing the long-term stability of the instrument. On a single orbit basis, SORCE SIM has an increase in temperature of about 1.7°C, whereas TSIS-1 SIM will increase by about 0.1°C.

Another consequence of SORCE SIM instrument power cycling concerns the operation of the ESR. The ESR is the only component in the SIM instrument that is actively temperature regulated. Detector heaters are located on the external shell of the detector and a second concentric shell provides additional thermal isolation to dampen any second order temperature gradients—see Harder, Lawrence, et al. (2005). Every-orbit power cycling induces a loss in temperature regulation and the ESR can no longer reach a stable operating temperature over the span of a single orbit. While phase sensitive detection allows for continued detector operation, additional thermal noise is generated and limits the stability of the observation particularly in the 1598.95–2401.4 nm spectral range. Additional operational constraints in the DO-Op mode also limit telemetry quality thereby substantially reducing the number of viable spectra that can be used in the SORCE TSIS-1 comparison for this wavelength range.

3. SORCE/TSIS-1 SIM Irradiance Scale Comparison

3.1. Matching Spectra

The comparison was conducted with SORCE SIM V27 and TSIS-1 SIM V06 (24-hr data product). The comparison was conducted from 23 March 2018 to 25 February 2020 spanning 705 days. During this time SORCE collected 684 observations and TSIS-1 conducted 563 observations. Observations from both instruments occurred on 579 common days. Small wavelength gaps in both the SORCE and TSIS-1 records are filled with valid data from the next valid time stamp (i.e., backfilling), and records with large wavelength gaps are rejected. The criterion for rejection is that if the day has more than 200 irradiance values missing, it is excluded. Sixteen (16) days were rejected for SORCE, and an additional nine (9) days were excluded due to missing TSIS-1 data, leaving a final sample of 554 days with concurrent and useable SORCE and TSIS spectra, thus ~79% of a daily cadence. Back-filled data at individual wavelengths is not included in calculating statistics for the comparison. Backfilled data are identified and flagged in data processing. Since the statistics are found one wavelength at a time, the number N_{mutual} in Equation set 1 could be different at each wavelength step.

The TSIS-1 SIM data is interpolated to match the SORCE SIM wavelength scale over the TSIS-1 SIM bandpass since the spectral sampling is slightly higher for TSIS-1. No wavelength scale shift or stretch was applied to the SORCE wavelength scale for this study. A wavelength shift/stretch is readily identifiable in two spectra by the appearance of derivative-like structure in the ratio with the spectral slope changes. There are small differences in the resolution of the two instruments due to small changes in dispersion of the prism glass and slight differences in figure of the optical elements. Improved scattered light rejection appears in the TSIS-1 SIM instrument due improved prism polishing capabilities and to the fact that all the photodiode detectors are placed 10 mm behind the exit slits for each channel whereas SORCE SIM instrument design allowed for 2 mm distance for the infrared and visible detectors, but with a 10 mm displacement behind the exit slit for the UV photodiode. For SORCE, the UV photodiode is located on the opposite side of the entrance slit from the ESR and the VIS1 and IR photodiodes. For TSIS-1 all the photodiode detectors are on the same side of the entrance slit as the ESR. Larger rotation angles are needed for the SORCE SIM in its configuration, and greater spectral overlap between the UV and visible photodiodes occurs for TSIS-1 SIM because of its position in the focal plane.

3.2. Comparison of SORCE and TSIS-1 SIM Spectra and Time Series

Figure 2a compares the spectra for SORCE V27 and TSIS-1 V06 SIM in the UV and includes the SORCE SOLSTICE V18 data (McClintock et al., 2005) convolved to the resolution of the SORCE SIM. The spectra shown in these plots is an average of 554 matched pairs and SOLSTICE had valid observations on each of the comparison days. Figure 2b shows the standard deviations for the individual instruments. Typically, a lower standard deviation occurs for TSIS-1 indicating improved stability and lower noise characteristics. Both SORCE and TSIS-1 SIM show smaller standard deviations than SOLSTICE most likely due to differences in the performance of

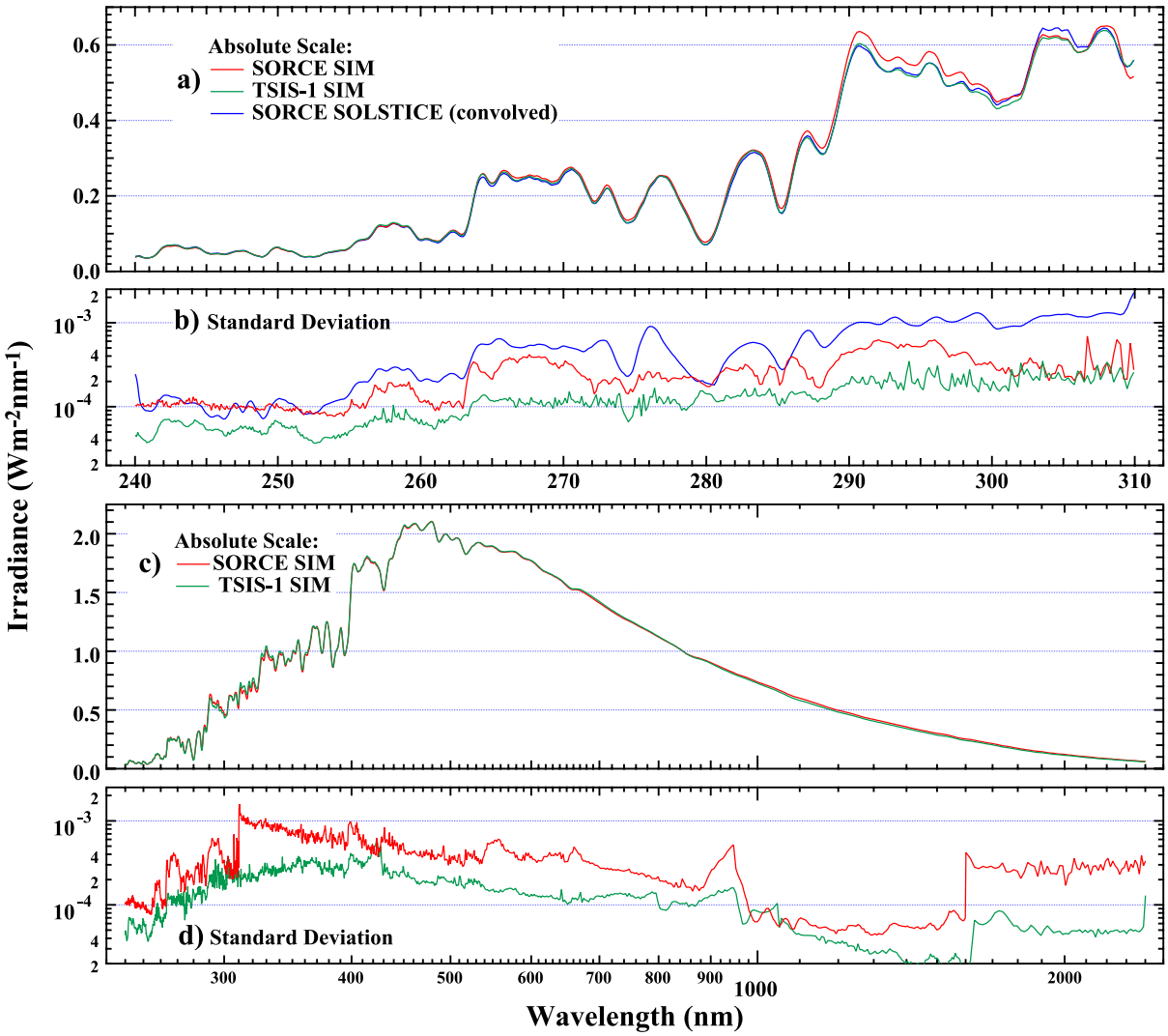

Figure 2. Comparison spectra for Solar Radiation and Climate Experiment (SORCE) V27 and Total and Spectral Irradiance Sensor (TSIS-1) V06 Spectral Irradiance Monitor (SIM). Panel (a) compares average SORCE SIM and Solar Stellar Irradiance Comparison Experiment (SOLSTICE) V18 with TSIS-1 SIM over the time span of the comparison. The SOLSTICE spectrum is convolved to the resolution of SORCE SIM. Panel (b) shows the standard deviations of each of these instruments. Panel (c) repeats this comparison for the full wavelength range of the SORCE and TSIS-1 SIM instruments. Panel (d) then gives the standard deviations for these two instruments.

photodiode detectors in the SIM instruments versus the SOLSTICE photomultiplier tubes with an additional contribution from temperature instability. Figures 2c and 2d repeat this for the full range of SORCE and TSIS-1 SIM. Deviations in the absolute scale appear in this figure, and will discussed in Section 3.3. As seen for the UV detectors, the visible and infrared standard deviations (Figure 2d) are smaller for TSIS-1 than SORCE. A lower signal-to-noise ratio (SNR) is apparent for SORCE SIM in the 310–400 nm range due to the limited performance of the sampling ADC. Also notable is increased noise for both instruments in the 880–1,000 nm range due to increased temperature coefficient for radiant sensitivity for silicon photodiodes. As discussed in Section 2.3.2, lower temperature stability significantly increases the standard deviation of the SORCE SIM ESR in the 1598.95–2401.4 nm range.

Figure 3 shows the time series for the instruments over the comparison time range at five different wavelengths with SOLSTICE included in the 250 nm panel. The differences in noise level are apparent in these plots with a high level of trend agreement throughout. The 1797.62 nm plot shows higher noise in the SORCE SIM ESR data. The open squares in this panel are the occasions of complete ESR infrared scans, the small closed squares are backfilled data.

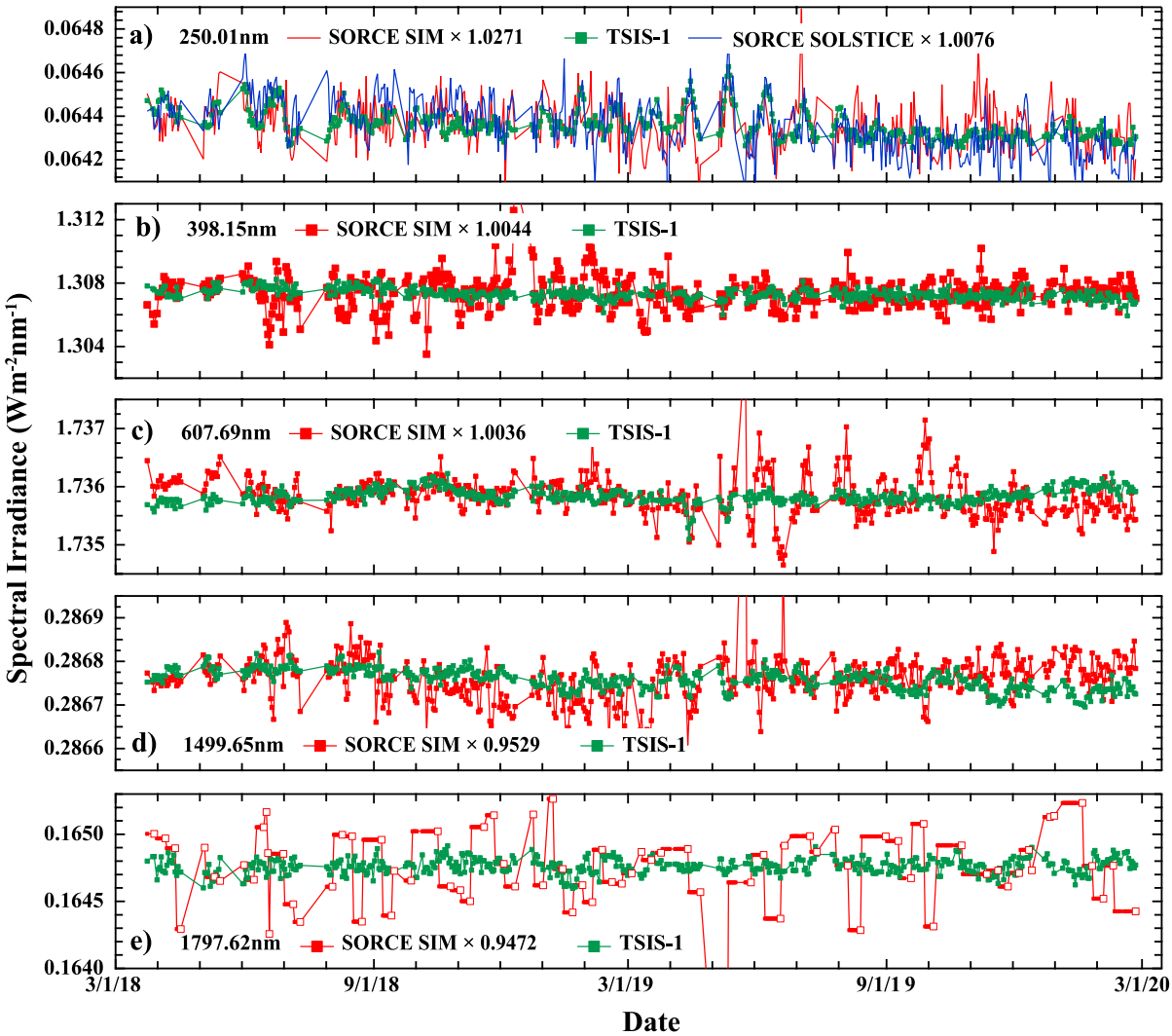

Figure 3. Selected time series of Solar Radiation and Climate Experiment (SORCE) V27 and Total and Spectral Irradiance Sensor (TSIS-1) V06 SIM data over the time span of the comparison for days with same time stamp. The SORCE Spectral Irradiance Monitor (SIM) V27 data has been scaled to match the TSIS-1 SIM mean irradiance, similar to the offset applied for TAV (see Section 4 for details).

3.3. Statistical Analysis of the SORCE and TSIS-1 SIM Spectra

The comparative analysis is conducted for both differences and ratios where the TSIS-1 SIM is viewed as the reference, thus the analysis shows deviations of SORCE relative to the TSIS-1 standard. The final correction factor will then be a wavelength dependent multiplicative vector that will bring the SORCE SIM irradiance scale into agreement with TSIS-1 SIM. This vector is referred to the STICR (SORCE-SIM to TSIS-1 SIM Irradiance Calibration Ratio) will be discussed in Section 4 later in this manuscript. Equations 1a–1g gives the basic statistical equations and are applied in subsequent subsections. The statistics are derived from 554 matched pairs of observations. For calculation of means for both ratio and difference, individual data points exceeding five standard deviations are rejected from the calculation and are clearly identifiable as spikes.

Because gaps in time appear in the mutual data set, the SORCE and TSIS-1 data are binned into 15-day intervals and averaged. This process allows for both suppression of random noise, and also allows for a more objective determination of the autocorrelation function. The 15-day binning reduces the number of samples in the comparison time period to 47 samples but guarantees at least two spectra appear in each consecutive bin. This bin averaging also excludes back-filled data. The median number of matched pairs in each bin is 13, with only five instances where the number of spectra in a single bin is less than or equal to five matched pairs.

$$\text{mean}_{\text{difference}}(\lambda) = \frac{\sum(\text{SORCE}(\lambda) - \text{TSIS}(\lambda))}{N_{\text{mutual}}(\lambda)} \tag{1a}$$

$$\text{mean}_{\text{ratio}}(\lambda) = \frac{\sum \frac{\text{SORCE}(\lambda)}{\text{TSIS}(\lambda)}}{N_{\text{mutual}}(\lambda)} \tag{1b}$$

$$\sigma^2_{\text{difference}}(\lambda) = \sigma^2_{\text{TSIS}} + \sigma^2_{\text{SORCE}} - 2\sigma^2_{\text{covariance}} \tag{1c}$$

$$\frac{\sigma^2_{\text{ratio}}(\lambda)}{\text{mean}^2_{\text{ratio}}(\lambda)} = \frac{\sigma^2_{\text{TSIS}}}{\overline{\text{TSIS}^2}} + \frac{\sigma^2_{\text{SORCE}}}{\overline{\text{SORCE}^2}} - 2\frac{\sigma^2_{\text{covariance}}}{\overline{\text{TSIS}} \times \overline{\text{SORCE}}} \tag{1d}$$

$$\sigma^2_{\text{covariance}}(\lambda) = \left\langle \frac{1}{N_{\text{mutual}}(\lambda)} \sum_i (\text{TSIS}_i - \overline{\text{TSIS}})(\text{SORCE}_i - \overline{\text{SORCE}}) \right\rangle \tag{1e}$$

$$\text{Error on mean}_{\text{difference or ratio}} = \frac{\sigma_{\text{difference or ratio}}}{\sqrt{N_{\text{mutual}}}} \sqrt{\frac{1+\varphi}{1-\varphi}} \tag{1f}$$

$$\varphi = \text{autocorrelation function}$$

$$\varphi(\lambda) = \frac{\sum_{k=0}^{M-L-1}(x_k - \bar{x})(x_{k+L} - \bar{x})}{\sum_{k=0}^{M-1}(x_k - \bar{x})^2} \quad (L = 1, M = 47 \text{ binned spectra}) \tag{1g}$$

$$\text{x} = \text{ratio or difference SORCE relative to TSIS}$$

Equations 1a–1g give the basic set of equations used to characterize the ratios and differences of SORCE relative to TSIS-1. In this way the comparative quantities show the deviations of SORCE relative to the TSIS-1 absolute standard. In Equation 1e, the bar over the TSIS-1 and SORCE values indicates the mean values calculated for the mutual 15-day binned SORCE and TSIS-1 data. Brackets surrounding the expression for the covariance in Equation 1e indicate a root-mean-square relation is imposed. In Equation 1g $M = 47$, the number of 15-day binned spectra.

3.3.1. SORCE and TSIS-1 SIM Autocorrelation As a Function of Wavelength

Figures 4a–4c) shows the SIM irradiance autocorrelation function as a function of wavelength for SORCE, TSIS-1 and the SORCE/TSIS-1 ratio, respectively. As noted in the previous section, the data is binned and averaged into 15-day blocks prior to computing the autocorrelation function; Figure 4c) integrates the data into 20 nm bins to suppress wavelength-to-wavelength contributions and overlays the data for comparison. The autocorrelation function combines many different aspects to both the performance of the instruments and to the nature of the 'light source' that the two instruments observe. Figures 4b and 4d show a systematically higher autocorrelation for the TSIS-1 instrument at almost all wavelengths relative to SORCE indicating a higher point-to-point stability in the wavelength dependence. The low autocorrelation values for SORCE (Figure 4a) are indicative of a more random point-to-point agreement. The structured SORCE autocorrelation is driven at some wavelengths by noise (such as in the 300–400 nm range) and at other wavelengths (500–600 nm range) by residual temperature variations not captured in the temperature dependent coefficient for radiant sensitivity for the photodiode detectors. The SORCE/TSIS-1 ratio (Figure 4c) tends to combine the characteristics of both instruments. The structure seen in autocorrelation plots is evident in the panels of Figure 3.

3.3.2. SORCE and TSIS-1 Difference and Ratio

Figure 5a shows the difference of SORCE relative to TSIS-1as a function of wavelength, the standard deviation and the standard error on the mean (SEM) difference (see Equations 1a, 1c, and 1f) are shown in Figure 5b. As in the calculation of the autocorrelation function (Section 3.3.1), the SORCE and TSIS-1 data are binned into the 15-day windows prior to calculating the difference. Also shown in Figure 5b is the SORCE SIM noise equivalent irradiance (NEI), essentially the detector noise limit that defines the ultimate precision achievable by this instrument. In Figure 5b the standard deviation of the difference does not exceed the 2σ value of the NEI, and except in the 280–310 nm range and the 700–800 nm range the SEM does not exceed 1σ value. In the 1,600–2,416 nm

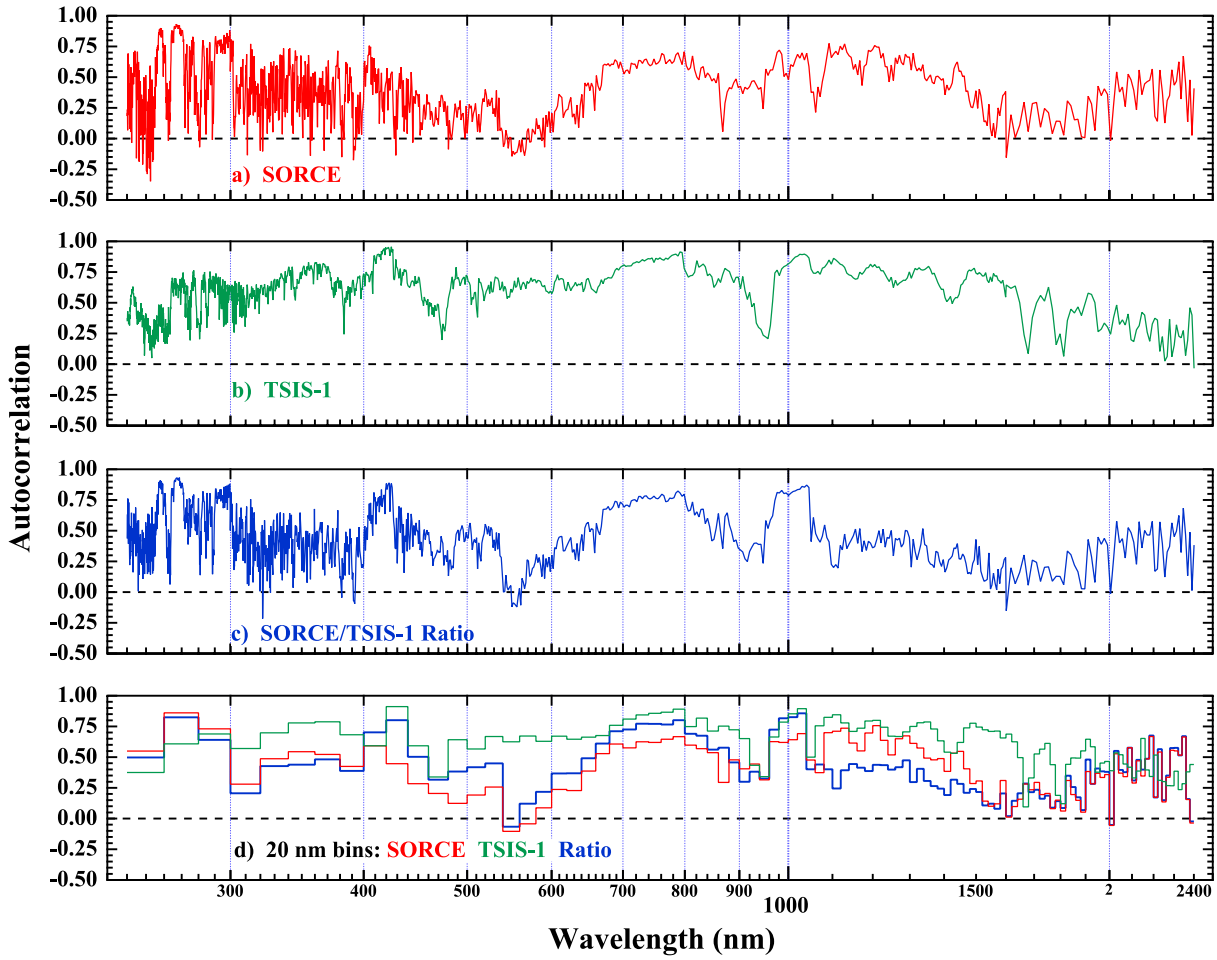

Figure 4. SIM irradiance autocorrelation as a function of wavelength. Panels (a–c) separately for Solar Radiation and Climate Experiment (SORCE), Total and Spectral Irradiance Sensor (TSIS-1), and the SORCE/TSIS-1 ratio, respectively. In all plots, the data are binned into 15-day blocks prior to computing the autocorrelation function. Panel (d) also integrates the data into 20 nm blocks to suppress fluctuations so the overall tendency of the autocorrelation can be observed.

range additional noise generated by temperature instability in SORCE increases the apparent noise seen in the ESR observations.

Figure 6 is analogous to Figure 5, but now for the fractional difference of SORCE relative to TSIS-1 SIM. Many of the same features appear in the ratio as seen in the difference; positive fractional differences in the UV photodiode in the 280–310 nm range, negative values in the 310–350 nm range, but the ratio shows different behavior in the infrared (950–2,416 nm) owing to a slowly changing decreases in irradiance difference with a continuously decreasing irradiance signal with increasing wavelength.

4. Production of the TSIS-1 SIM Adjusted Values (TAV V02)

The publicly available analysis for TAV V02 is derived and documented in a data set called STICR (SORCE SIM to TSIS-1 SIM Irradiance Calibration Ratio). The STICR is the mean TSIS-1/SORCE SIM irradiance ratio during the temporal overlap presented in this manuscript. The STICR SORCE and TSIS-1 mean spectra, plus all ancillary data needed to understand how this ratio was derived are contained in this data product. STICR V02 is used to create V02 of the SORCE SIM TAV irradiance data product. See Section 6 on data access for the relevant URL links.

In simple terms, the SORCE-SIM TAV irradiance given by Equation 2:

$$\mathrm{SORCE}_{\mathrm{irradiance}} \times \mathrm{STICR} = \mathrm{SORCE\_TAV}_{\mathrm{irradiance}} \quad (2)$$

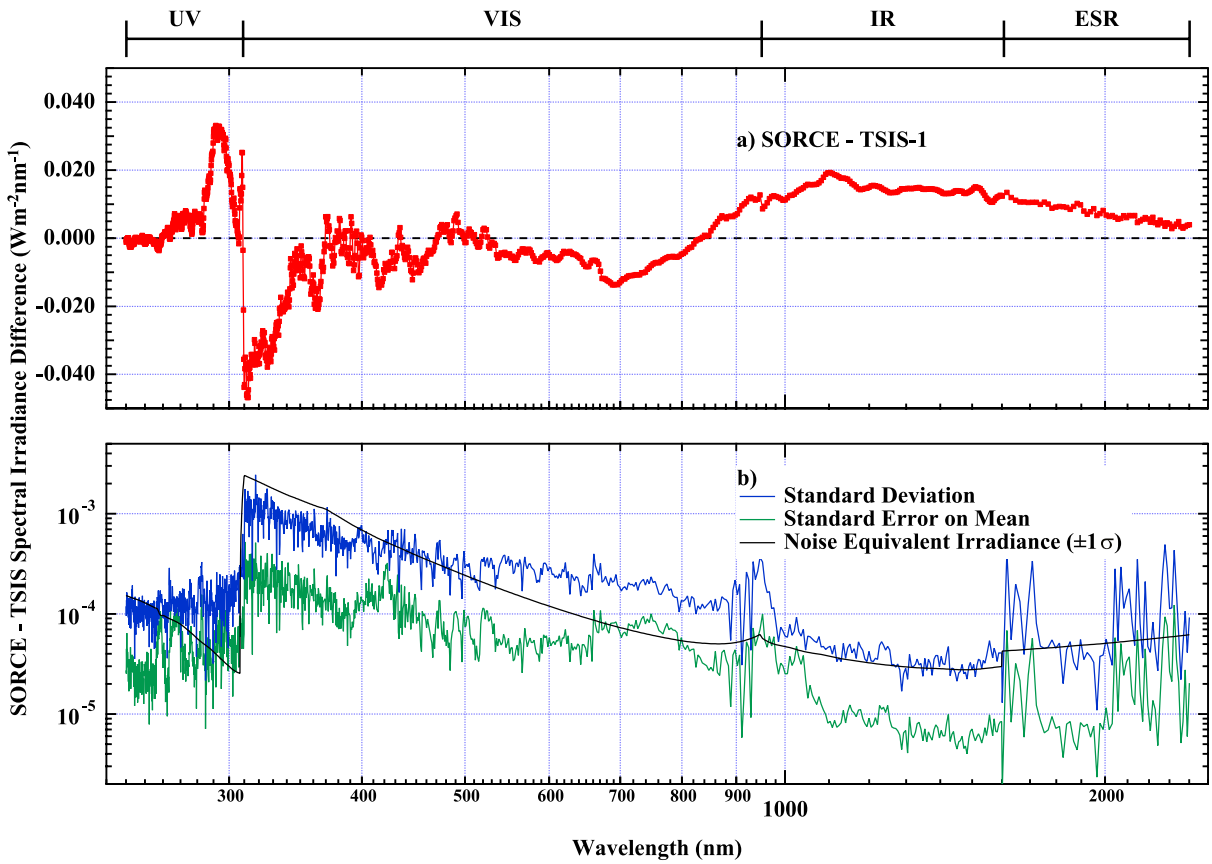

Figure 5. Panel (a) shows the spectral irradiance difference of Solar Radiation and Climate Experiment (SORCE) relative to Total and Spectral Irradiance Sensor Spectral Irradiance Monitor averaged over the 47 15-day blocks. Panel (b) give the standard deviation, standard error on the mean (SEM), and the noise equivalent irradiance for the UV, VIS, and IR photodiodes for the 240.02–1,600 nm range and the electrical substitution radiometer measurements in the 1,598.95–2,401.4 nm range. Except for the 280–310 nm region and 700–800 nm range, the SEM does not exceed the ±1σ instrument noise level – thus the difference is mostly noise limited. The top bar on the plot indicates which SORCE detector is used for the observation.

Figure 7a shows the STICR as it appears in the STICR data file discussed in the previous paragraph. Figure 7a shows the full spectral range on a log-wavelength scale. While either differences or ratios can be used to perform the correction of SORCE to match TSIS-1, the ratio as expressed in Equation 2 was selected to remain consistent with the way the SORCE SIM irradiance scale factor (ALEPH) was derived in Section 4.3 of Harder et al. (2010).

Version 27 SORCE SIM data provides a daily time dependent uncertainty based on SIMA-to-SIMB differences (Harder et al., 2021). TSIS-1 SIM decomposes its uncertainty into three components: (a) the pre-launch calibration uncertainty based on component level characterizations and end-to-end spectral validation (Richard et al., 2020); (b) measurement precision based on scan-to-scan repeatability (equivalent to the SORCE NEI discussed in Section 3.3.2); (c) Measurement uncertainty associated with degradation corrections and observed differences from the three independent channels. The TSIS-1 measurement uncertainty is then the quadrature addition of precision and measurement uncertainty and reflects the actual uncertainty associated with on-orbit measurements and is equivalent to the quoted SORCE uncertainty.

Equation 3 is analogous to Equations 1b–1g we can write the STICR and the ratio error $\mathrm{STICR}_{\mathrm{err}}$ to derive the uncertainty on the $\mathrm{STICR}_{\mathrm{unc}}$:

$$\mathrm{STICR}(\lambda) = \frac{\mathrm{TSIS}_{\mathrm{irrad}}(\lambda)}{\mathrm{SORCE}_{\mathrm{irrad}}(\lambda)} \tag{3a}$$

$$\frac{\mathrm{STICR}_{\mathrm{err}}(\lambda)}{\mathrm{STICR}(\lambda)} = \sqrt{\left(\frac{\mathrm{SORCE}_{\mathrm{unc}}(\lambda)}{\mathrm{SORCE}_{\mathrm{irrad}}(\lambda)}\right)^2 + \left(\frac{\mathrm{TSIS}_{\mathrm{unc}}(\lambda)}{\mathrm{TSIS}_{\mathrm{irrad}}(\lambda)}\right)^2 - \frac{2 \times \mathrm{STICR}_{\mathrm{covariance}}(\lambda)}{\mathrm{TSIS}_{\mathrm{irrad}}(\lambda) \times \mathrm{SORCE}_{\mathrm{irrad}}(\lambda)}} \tag{3b}$$

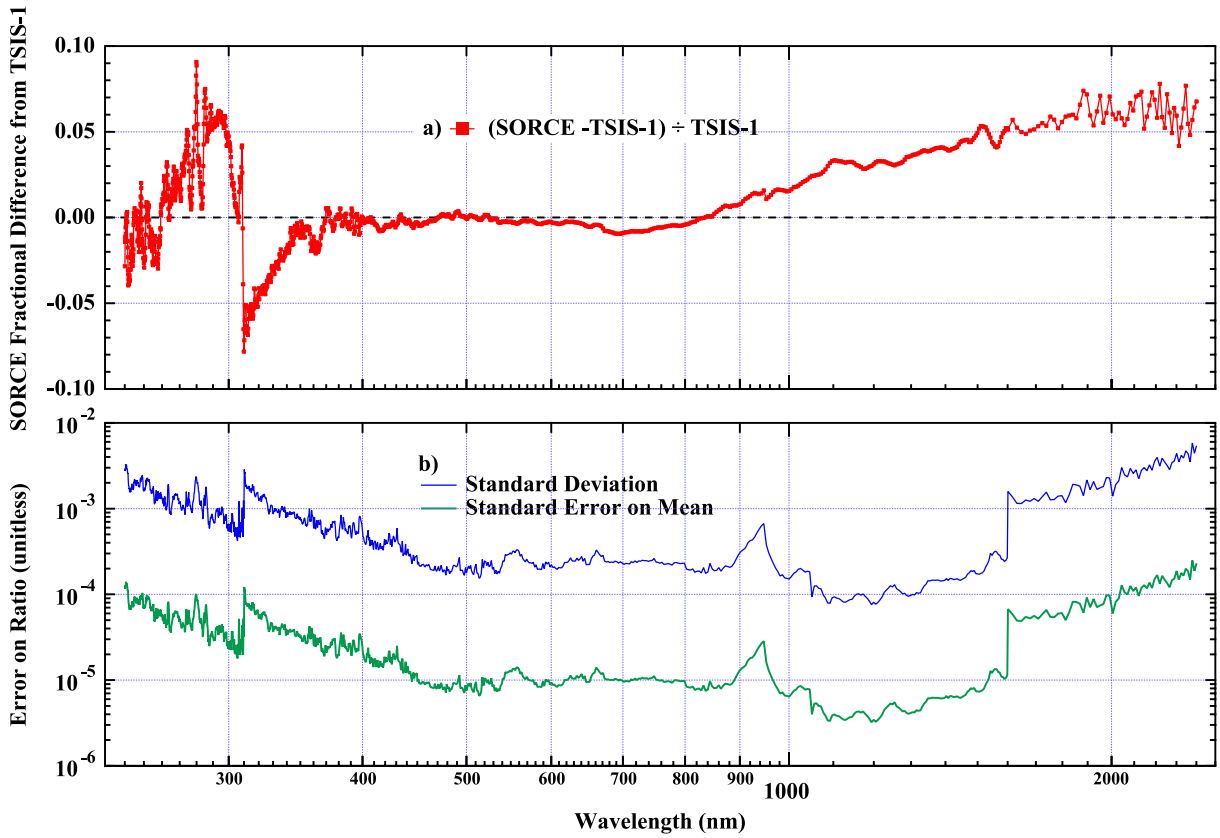

Figure 6. Panel (a) shows the fractional difference of Solar Radiation and Climate Experiment Spectral Irradiance Monitor (SIM) V27 relative to Total and Spectral Irradiance Sensor V06 SIM. Panel (b) gives the standard deviation and standard error on the mean on the ratio.

$$\mathrm{STICR}_{\mathrm{unc}}(\lambda) = \frac{\mathrm{STICR}_{\mathrm{err}}(\lambda)}{\sqrt{N_{\mathrm{mutual}}}} \sqrt{\frac{1+\varphi}{1-\varphi}} \tag{3c}$$

We investigated the effects of smoothing the TAV ratio shown in Figure 7a with a b-spline function and found a significantly reduced level of agreement between the two instruments. It is likely that differences in the two spectrometer's dispersion and possible scattered light contributions in SORCE produce the structure seen in Figure 7a. To suppress this wavelength structure all three panels of Figure 7 show a spectral binning of 10 nm for the 240 nm to 1,600 spectral range and a wider 40 nm binning for the 1,600 nm–2,400 nm range to accommodate the lower spectral sampling of the ESR.

Figures 7b and 7c simulate the effects of reduced comparison time on the ability to produce the STICR correction factor. Figure 7b shows the fractional difference from the full 704-day comparison in blocks of increasing time duration from 176 to 528 days. The same procedures were followed in producing the shorter comparison records as was done for the full 704-day analysis. The fractional differences in the determination of STICR relative to the full 704-day comparison show larger scatter in the UV variations but dampened with increasing length of comparison. Except for the first 176-day time period, the 352- and 528-day comparison length records fall within a ±500 ppm agreement level with the 704-day record. Similarly, for wavelengths greater than 1,600 nm, the decreased level of stability produces larger and less organized agreement with the full time period comparison. For the 400–1,600 nm range, the different lengths of overlap time are considerably less important with less than about 250 ppm variations from the full record. As expected, in Figure 7c the standard error on the mean systematically improves with the length of time for the comparison. It is important to characterize the impact of the length of overlap from the perspective of both mission planning and the scientific impact of stability of long-term records. For the determination of an absolute irradiance correction factor, a reduced overlap campaign time of 6–12 months is acceptable for the visible and near IR regions, but for the UV and the infrared >1,600 nm a length

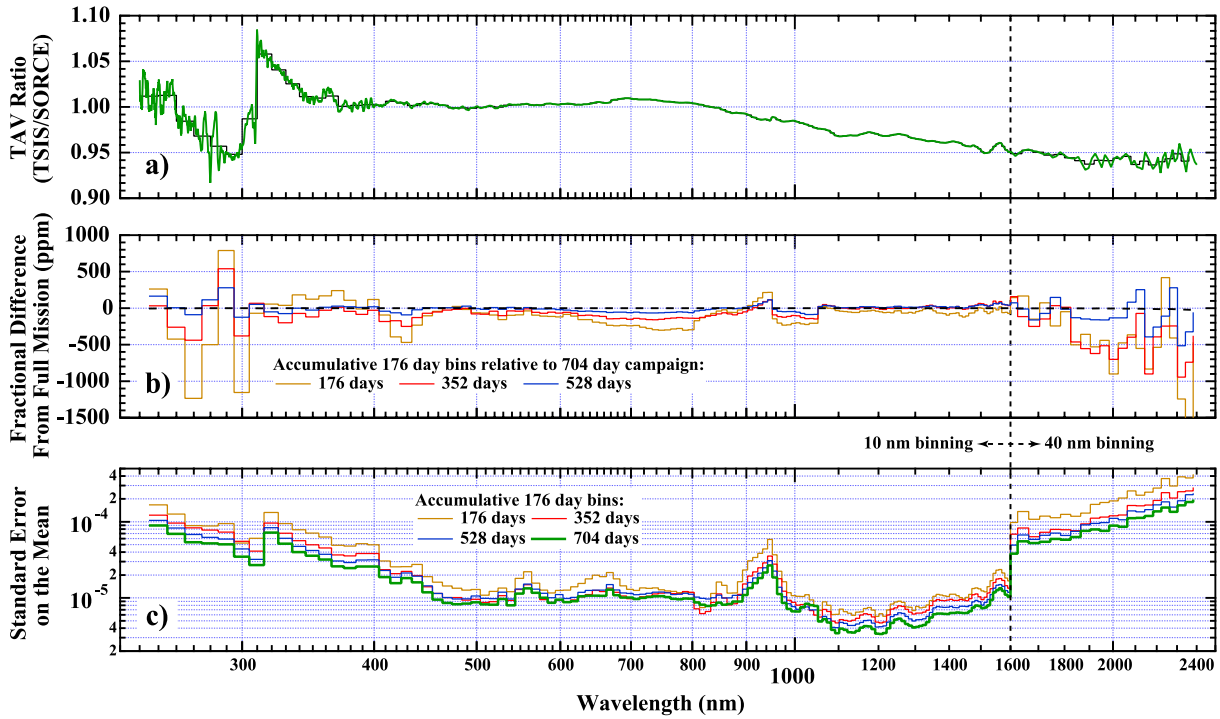

Figure 7. The Solar Radiation and Climate Experiment (SORCE) TSIS-1 Irradiance Calibration Ratio (STICR). STICR is a multiplicative factor that brings the SORCE V27 data onto the absolute calibration scale of Total and Spectral Irradiance Sensor (TSIS-1). Panel (a) shows the STICR-V2.0 correction factor, shown in green for the standard SORCE Spectral Irradiance Monitor wavelength scale. Panels (b) and (c) simulate the effects of shorter overlap campaigns relative to the 704 days overlap experiment shown in this study. This is done for both fractional differences (b) and for the standard error on the mean (c). All three panels also show a 10 nm spectral binning for 240–1,600 nm and 40 nm binning in the 1,600–2,400 nm region to suppress wavelength-to-wavelength structure. See the text for further discussion.

of overlap of about 1 year is more appropriate. An overlap of 1 year allows for the characterization instrument behavior over the full range of on-orbit temperature variations and changes in optical behavior caused by ~7% change in the apparent solar intensity with the Earth's elliptical orbit.

It must be emphasized that the discussion in the previous paragraph relates to the length of time required to produce an absolute scale correction factor. However, an equally important analysis of long-term stability is needed to address stability in multi-satellite data records. A more detailed analysis on this topic is in preparation for this journal and will be published in 2022. The salient points of this second manuscript will include discussion of (a) how autocorrelation affects the ability to identify real trends in the data; (b) non-linear behavior associated with transient response in one or both instruments cannot be mis-interpreted as a long-term trend; and (c) the ability to detect long-term trends is highly dependent on the length of overlap. This study will be conducted as a function of wavelength and will expand the discussion found in Weatherhead et al. (2017) and apply the methodology advocated in Weatherhead et al. (1998).

5. Integrated SORCE TAV V02 Spectral Irradiance Relative to SORCE TIM V19

The greatest value of the SORCE and TSIS-1 SIM instruments is the broad wavelength coverage amounting to about 96% of the total radiated output of the Sun thereby providing the ability to decompose the TSI and determine the wavelength dependent contributions to the total as well as the wavelength contributions to variability. Section 3.3.2 gave the spectral irradiance difference and ratio between SORCE and TSIS-1. The integrated SORCE and TSIS-1 instruments give a mean integrated SSI (ISSI) of 1321.17 ± 0.91 and 1308.43 ± 0.06 W m^{-2}, respectively. The SORCE-TSIS-1 ISSI difference is 12.834 ± 0.191 W m^{-2} with a SORCE/TSIS-1 ratio of 1.0098 ± 0.00015. The application of the $STICR_{tav\_ratio}$ (Equation 2) then corrects SORCE to the TSIS-1 calibrated values and produces the TAV value that can be compared to the TSI over the full extent of the SORCE mission.

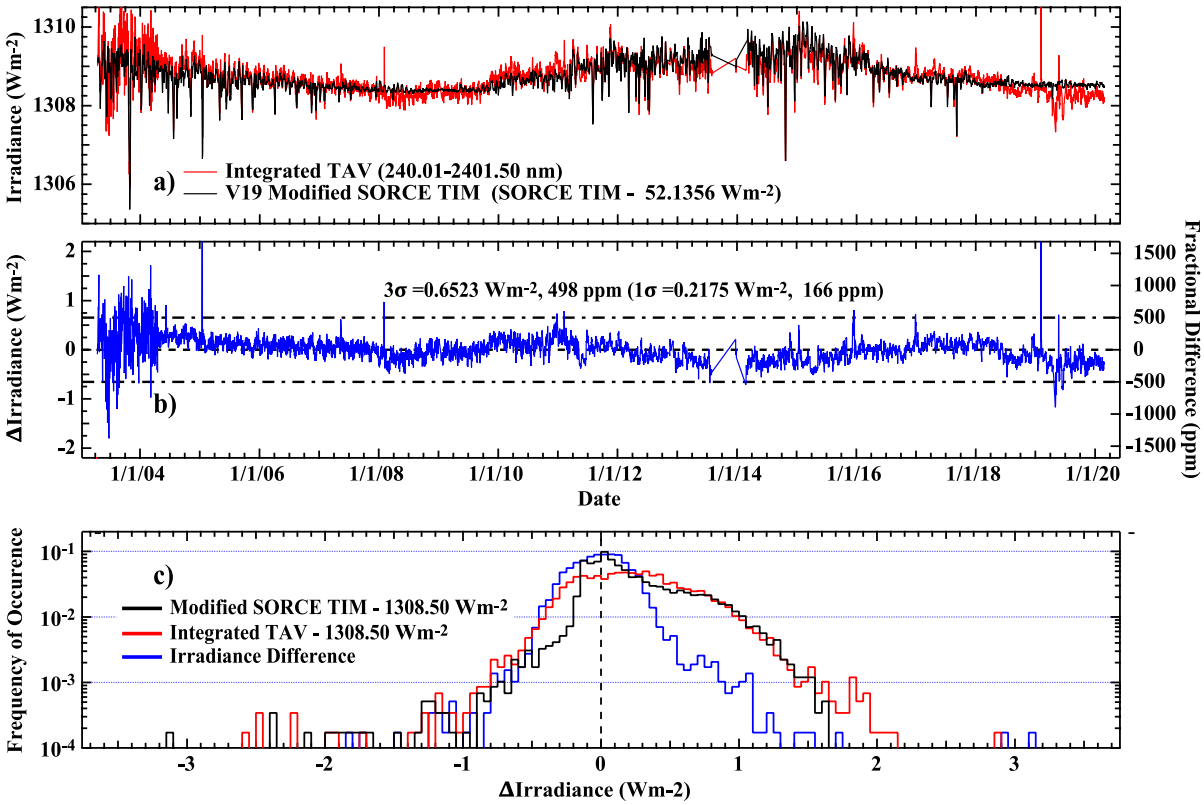

Figure 8. A comparison of Solar Radiation and Climate Experiment TSIS-1 Spectral Irradiance Monitor (SIM) Adjusted Value Integrated solar spectral irradiance (SORCE TAV ISSI) to the TSI as measured by SORCE SIM. Panel (a) compares the integrated SIM relative to the modified TSI value defined as SORCE TIM V19–52.1356 W m^{-2}. Panel (b) then displays the SORCE TAV ISSI-modified TSI difference between the time series of panel (a) with absolute difference on the left-hand axis, with fractional differences in parts per million on the right. Panel (c) shows frequency of occurrence histograms versus the change in irradiance. See the text for discussion on this panel.

The TSI gives the total radiated power, but for the spectral measurements approximately 96% of the TSI can be addressed through spectral irradiance integration in the 240–2,416 nm region. Over the full length of the SORCE mission, the residual unmeasured part of the spectrum amounts to a 52.1356 ± 0.217 W m^{-2} deficit. Figure 8 details the comparison of TAV ISSI and SORCE TIM TSI (Kopp et al., 2005). As explained in the previous section, TAV ISSI is generated by integration of the SORCE SIM TAV data product. Figure 8a compares the time series of TAV ISSI and with the modified TSI defined as SORCE TIM V19–52.1356 W m^{-2} Figure 8b gives the residual difference and includes ±3σ error limits of 0.653 W m^{-2}.

In Figure 8c, the TAV ISSI and modified TSI histograms constructs the frequency of occurrence versus change in irradiance relative to the most probable irradiance (i.e., the mode of the distribution), a value indicated as 1308.50 W m^{-2} within a bin size of 0.05 W m^{-2}. The blue trace Figure 8c then shows the histogram using the residual difference displayed in Figure 8b. Figure 8c then relates the distribution in changes in irradiance of the TSI and ISSI over the solar cycle relative to the magnitude of the mismatch between the two measurements. Figure 8c shows a number of interesting results related to both the nature of the variability and the instruments that measure this variability. For ISSI and TSI the distributions are highly non-Gaussian with significant contributions from higher moments of the distribution (skew and kurtosis.) Most notably the TSI measurement is leptokurtic and the integrated SSI is platykurtic; the most probable TSI has a populated about a factor of 2 greater than flat-toped and more broadly distributed ISSI. The TSI and ISSI tend to track each other for more positive values, but for negative values the ISSI shows a greater population of values indicating a greater number of negative deviations in excess of decreases associated with dark solar features like sunspots. The difference histogram is more Gaussian in nature, with a full width half maximum of 0.5 W m^{-2}, standard deviation of 0.212 W m^{-2} in agreement with the quoted value in Figure 8b. The higher noise levels in the first 450 days of the time series seen in Figure 8b are caused by poor wavelength control for the ESR in the 1598.95–2401.4 nm range that was corrected after that time

period. Conducting the same analysis excluding the first 450 days reduces the standard deviation to 0.207 W m^{-2}. In a similar manner, the decrease in the ISSI signal after June of 2018 is related to temperature effects in the ESR as noted in Section 2.3.2 and shown most clearly in Figure 8b.

Outside the integrated wavelength range of Figure 8, the integrated irradiance from 200 to 240 nm contributes an additional 1.382 ± 0.004 W m^{-2} (average of SORCE SOLSTICE and TSIS-1 SIM); the SOLSTICE FUV portion (115–200 nm) adds 0.0996 ± 0.0004 W m^{-2}. Altogether, the most reliable integrated SSI gives 1309.91 W m^{-2} thereby giving an apparent contribution of 50.77 W m^{-2} attributable to the infrared longward the 2401.4 nm measured spectrum relative to SORCE TIM. Note that TSIS-1 TIM reports a TSI value of 0.858 W m^{-2} higher than SORCE TIM over the overlap time stamps reported in this paper.

6. Data Access

This comparison was conducted using the publicly available SORCE SIM V27 and TSIS-1 SIM V06 (24-hr) datasets. STICR V02 (STICR = SORCE SIM to TSIS-1 SIM Irradiance Calibration Ratio) and TAV V02 (TAV = TSIS-1 Adjusted Values) also use the same data releases. The DOIs for the datasets used are:

1. SORCE V27: https://doi.org/10.5067/LDDKZ3PXZZ5G.
2. TSIS V06: https://doi.org/10.5067/TSIS/SIM/DATA312.
3. STICR V02: https://doi.org/10.25810/22v9-9s08.
4. TAV V02: https://doi.org/10.5067/8E8EG9HHVDZS.

The TSIS-1 SIM data is available at: https://lasp.colorado.edu/home/tsis/data/ssi-data/, and the SORCE (SIM and TAV) datasets are available at https://lasp.colorado.edu/home/sorce/data/. All three are also available at the NASA DAAC, https://disc.gsfc.nasa.gov/datasets/.

The STICR V02 data product is housed at CU Scholar—a collaborative service of the University of Colorado Libraries, and is available in ASCII and IDL. SAV file format. Version notes on STICR are also available at this site.

More information on the Interactive Data Language (IDL) is available at: https://www.l3harrisgeospatial.com/Software-Technology/IDL.

An IDL file reader is available at: http://lasp.colorado.edu/data/sorce/file_readers/read_lasp_ascii_file.pro.

This program will read the ASCII files and return an array of IDL structures. The STICR IDL SAV file contains all the information in the ASCII file, plus additional information such as the specific days during the SORCE and TSIS-1 temporal overlap which were used in the determination of the STICR.

7. Conclusions and Discussion

The analysis presented in this paper can be summarized in the following way:

1. Advancements in pre-flight calibration capabilities make the TSIS-1 SIM calibration more accurate by about an order of magnitude over what was available during the SORCE pre-flight era. Thus, a correction to the absolute scale is a justifiable activity. In essence, this comparison provides an on-orbit calibration of the SORCE instrument with TSIS-1 SIM acting as a radiometric transfer standard from a NIST-calibrated cryogenic radiometer compliant with international standards (Richard et al., 2020).
2. The comparison was conducted on two instruments in entirely different states of stability and degradation. The reduced temperature stability of the SORCE SIM added additional systematic noise to the reported measurement particularly for the infrared greater than 1598.95 nm as measured by the ESR. In spite of the reduced stability, the standard deviation of ratios and differences were typically within the 2σ noise limit of the SORCE SIM detectors.
3. The SORCE-SIM to TSIS-1 SIM Irradiance Calibration Ratio (STICR V02) has been applied to SORCE SIM V27 to create the TSIS-1 Adjusted Values (TAV V02). The STICR data product, which provides all the intermediary data, is publicly available as described in Section 6.
4. Comparing the TAV V02 values to SORCE TIM V19, it is found that the 1σ standard deviation is 0.2175 W m^{-2} or 166 parts per million, a remarkable success for a first-generation instrument.

The methodology reported in this manuscript demonstrates that on-orbit recalibration can be very accurately conducted for two instruments with a well-matched and characterized optical/electrical/mechanical design. The advancements in SIRCUS-based (i.e., tunable lasers stimulation + cryogenic radiometer reference) will continue to lead the way for reproducible and tracible preflight calibrations. Future common TSIS-1 and TSIS-2 SIM instrument design and in-flight re-calibration will allow for the concatenation of multi-satellite time series of SSI with lower uncertainties than those found in this analysis.

Conflict of Interest

The authors declare no conflicts of interest relevant to this study.

Data Availability Statement

The special data sets developed specifically for the content of this manuscript and described in Section 6 are served through CU Scholar—a collaborative service provided by the University of Colorado Libraries.

Acknowledgments
This research was supported by the NASA Solar Radiation and Climate Experiment, contract NAS5-97045, and Solar Irradiance Science Team (SIST-2), Award 80NSSC18K1306. We would also like to thank two anonymous reviewers for suggestions that improved the manuscript.

References

Austin, J., Tourpali, K., Rozanov, E., Akiyoshi, H., Bekki, S., Bodeker, G., et al. (2008). Coupled chemistry climate model simulations of the solar cycle in ozone and temperature. *Journal of Geophysical Research*, *113*, D11306. https://doi.org/10.1029/2007JD009391

Brown, S. W., Eppeldauer, G., Rice, J. P., Zhang, J., & Lykke, K. (2004). Spectral Irradiance and Radiance Responsivity Calibrations using Uniform Sources (SIRCUS) facility at NIST. In W. L. Barnes, & J. J. Butler (Eds.), *Earth observing systems* (p. 363). SPIE Conf. Series 5542. https://doi.org/10.1117/12.559577

Dhomse, S. S., Chipperfield, M. P., Damadeo, R. P., Zawodny, J. M., Ball, W. T., Feng, W., et al. (2016). On the ambiguous nature of the 11 year solar cycle signal in upper stratospheric ozone. *Geophysical Research Letters*, *43*, 7241–7249. https://doi.org/10.1002/2016GL069958

Douglass, D. H., & Clader, B. D. (2002). Climate sensitivity of the Earth to solar irradiance. *Geophysical Research Letters*, *29*, 33-1–33-4. https://doi.org/10.1029/2002GL015345

Forster, P., Ramaswamy, V., Artaxo, P., Berntsen, T., Betts, R., Fahey, D., et al. (2007). Changes in atmospheric constituents and in radiative forcing. In *Climate change 2007: The physical science basis. Contribution of working group I to the Fourth assessment report of the Intergovernmental Panel on Climate Change*. Cambridge University.

Gray, L. J., Beer, J., Geller, M., Haigh, J. D., Lockwood, M., Matthes, K., et al. (2010). Solar influences on climate. *Review of Geophysics*, *48*, RG4001. https://doi.org/10.1029/2009RG000282

Harder, J. W., Beland, S., Penton, S., Sandoval, L., Mothersbaugh, J., & Woods, T. N. (2021). *Algorithm theoretical basis document – post launch update: Spectral Irradiance Monitor (SIM)*. https://doi.org/10.25810/rff8-ff38

Harder, J. W., Fontenla, J. M., Lawrence, G., Woods, T. N., & Rottman, G. J. (2005). The spectral irradiance monitor: Measurement equations and calibration. *Solar Physics*, *230*(1-2), 169–204. https://doi.org/10.1007/s11207-005-1528-1

Harder, J. W., Lawrence, G., Fontenla, J., Rottman, G. J., & Woods, T. N. (2005). The Spectral Irradiance Monitor: Scientific requirements, instrument design, and operation modes. *Solar Physics*, *230*, 141–167. https://doi.org/10.1007/s11207-005-5007-5

Harder, J. W., Thuillier, G., Richard, E. C., Brown, S. W., Lykke, K. R., Snow, M., et al. (2010). The SORCE SIM solar spectrum: Comparison with recent observations. *Solar Physics*, *263*(1-2), 3–24. https://doi.org/10.1007/s11207-010-9555-y

Kopp, G., Lawrence, G., & Rottman, G. (2005). The total irradiance monitor (TIM): Science results. *Solar Physics*, *230*, 129–139. https://doi.org/10.1007/s11207-005-7433-9

Mattthes, K., Funke, B., Anderson, M. E., Barnard, L., Beer, J., Charbonneau, P., et al. (2017). Solar forcing for CMIP6 (v3.2). *Geoscientific Model Development*, *10*, 2247–2302. https://doi.org/10.5194/gmd-10-2247-2017

McClintock, W. E., Rottman, G. J., & Woods, T. N. (2005). Solar-stellar irradiance comparison experiment II (SOLSTICE II): Instrument concept and design. *Solar Physics*, *230*, 225–294. https://doi.org/10.1007/s11207-005-1585-5

Mitchell, D. M., Gray, L. J., Fujiwara, M., Hibino, T., Anstey, J., Harada, Y., et al. (2015). Signatures of naturally induced variability in the atmosphere using multiple reanalysis datasets. *The Quarterly Journal of the Royal Meteorological Society*, *141*, 2011–2031. https://doi.org/10.1002/qj.2492

Richard, E., Harber, D., Coddington, O., Drake, G., Rutkowski, J., Triplett, M., et al. (2020). SI-traceable spectral irradiance radiometric characterization and absolute calibration of the TSIS-1 spectral irradiance monitor (SIM). *Remote Sensing*, *12*, 1818. https://doi.org/10.3390/rs12111818

Seppälä, A., & Clilverd, M. A. (2014). Energetic particle forcing of the Northern Hemisphere winter stratosphere: Comparison to solar irradiance forcing. *Frontiers in Physics*, *2*, 25. https://doi.org/10.3389/fphy.2014.00025

Thuillier, G., Foujols, T., Bolsée, D., Gillotay, D., Hersé, M., Peetermans, W., et al. (2009). SOLAR/SOLSPEC: Scientific objectives, instrument performance and its absolute calibration using a blackbody as primary standard source. *Solar Physics*, *257*(1), 185–213. https://doi.org/10.1007/s11207-009-9361-6

Weatherhead, E. C., Harder, J. W., Araujo-Pradere, E. A., Bodeker, G., English, J. M., Flynn, L. E., et al. (2017). How long do satellites need to overlap? Evaluation of climate data stability form overlapping satellite records. *Atmospheric Chemistry and Physics*, *17*, 15069–15093. https://doi.org/10.5194/acp-17-15069-2017

Weatherhead, E. C., Reinsel, G. C., Tiao, G. C., Meng, X., Choi, D., Cheang, W.-K., et al. (1998). Factors affecting the detection of trends: Statistical considerations and applications to environmental data. *Journal of Geophysical Research*, *103*(D14), 17149–17161. https://doi.org/10.1029/98JD00995